IEEE Access
Multidisciplinary ⋮ Rapid Review ⋮ Open Access Journal

Received December 13, 2020, accepted December 25, 2020, date of publication December 30, 2020,
date of current version January 8, 2021.

Digital Object Identifier 10.1109/ACCESS.2020.3047961

Three-Phase UPQC Topology Based on Quadruple-Active-Bridge

JIAN HAN, XING LI, YAN JIANG, AND SHAONAN GONG
College of Electrical and Information Engineering, Hunan University, Changsha 410082, China

Corresponding author: Xing Li (lxhnu@hnu.edu.cn)

This work was supported by National Key Research and Development Project of China under Grant 2018YFB0606000.

ABSTRACT In this study, a three-phase unified power quality conditioner (UPQC) topology based on a quadruple-active-bridge (QAB) is presented as an attractive solution to power quality issues. It is composed of three single-phase series converters, a three-phase shunt converter and a QAB converter located at the common DC-link. Since the bulky low frequency isolation transformers are replaced by the high frequency ones in QAB, it leads to higher power density, reduced weight and volume. The QAB converter could function as an energy router to provide multiple DC-link voltage access ports in the UPQC, which increase the flexibility of the UPQC. Finally, the MATLAB/Simulink simulation results and hardware-in-the-loop testing verify the correctness and effectiveness of the proposed topology and control method.

INDEX TERMS Unified power quality conditioner (UPQC), quadruple-active-bridge (QAB), power quality, power electronics, adaptive filter.

I. INTRODUCTION

Nowadays, the power quality (PQ) issues, including reactive and harmonic currents, sags/swells in the supply voltage, and distortion, are critical and not new [1], [2]. Especially, with the growing use of renewable energy sources (RES), such as inverter-based large-scale photovoltaic (PV) and wind integration, distributed generator (DG) system, vehicle to grid (V2G), the power quality issues become more severe [3]–[6].

In order to overcome those PQ issues, many power electronics-based compensation devices, such as static var generator (SVG), active power filter (APF) [7], [8], dynamic voltage restorer (DVR) [9], [10], unified power quality conditioner (UPQC) [11]–[13], are developed. Among these compensation devices, the topology of UPQC is relatively complex, which is formed with the back-to-back connection of a series-APF and a shunt-APF through a common DC-link. However, the UPQC is still considered as the most potential and versatile compensation device [13], because it possesses the ability of alleviating almost all the voltage- and current-related PQ issues.

Currently, many researchers have done a lot to study the topologies of UPQC with different aims [13]. In [14], [15], the UPQC integrated with DG system (UPQC-DG) is presented to relieve the load active power demand on the grid, while the investment cost is relatively high. In [16], the interline UPQC (UPQC-I) is proposed to control the active power flow between two feeders and mitigate the PQ issues of the two feeders, but the current- and voltage-related PQ issues are not simultaneously mitigated in the same feeder. To improve the power level of UPQC, the modular UPQC [17], [18] based on cascade H-bridge and multilevel UPQC are proposed. To reduce the number of switches, a novel ten-switch topology for UPQC are proposed [19]. Although the UPQC with less switches has the advantages of decreased investment cost, it will inevitably increase DC-link voltage level. To avoid the use of transformers, the single-phase transformer-less UPQC and three-phase UPQC made up of three single-phase UPQCs (TSP-UPQC) without series transformers are proposed in [27] and [28], but the unbalanced grid currents cannot be compensated when mitigating the unbalanced grid voltage [28]. In [20], [21], some attention is put on the UPQC integrated with dual-active-bridge (DAB). The UPQC-DAB has the advantages of reduced cost, volume and weight, because the bulky low frequency (LF) isolation transformers are replaced by the high-frequency (HF) ones. However, in the DAB based TSP-UPQC, the unbalanced grid currents cannot be mitigated under unbalanced load, because it is not possible to realize the transfer of energy among each phase [21].

In this study, a quadruple-active-bridge (QAB) [22]–[24] based UPQC is proposed, which is formed with the

The associate editor coordinating the review of this manuscript and approving it for publication was Nagesh Prabhu.

TABLE 1. Comparison with the existing topologies.

	Removing LF transformer	Number of DC power electronics interfaces	Voltage sag/swell mitigation	Reactive power compensation	Current harmonics elimination	Unbalanced grid current mitigation
Three-phase DVR	×	1	√	√	×	√
TSP-DVR	×	3	√	√	×	×
Three-phase STATCOM	×	1	×	√	√	√
Three-phase UPQC	×	1	√	√	√	√
TSP-UPQC	×	3	√	√	√	×
Three-phase UPQC-DAB	×	2	√	√	√	√
Three-phase UPQC- QAB	√	4	√	√	√	√

back-to-back connection of three single-phase series converters and a three-phase converter through a QAB converter. Due to the lack of the bulky low frequency isolation transformers, the proposed UPQC-QAB has higher power density, reduced cost, volume and weight. Because the QAB converter functions as an energy router in the UPQC, it cannot only provide more power electronic interfaces for renewable energy sources, but also make it possible to mitigate the unbalanced grid currents caused by the unbalanced load. Besides, compared with DAB based TSP-UPQC, the number of switches and DC-link capacitances can be reduced. Although the three-phase UPQC-DAB could also remove the bulky low frequency isolation transformers, it could not provide more power electronic interfaces (only two DC ports) [29].

In summary, the main contributions of this study include:

- ✓ A three-phase UPQC topology based on the QAB is proposed, which can improve the power density and flexibility;
- ✓ The UPQC-QAB not only has the same functions as a conventional UPQC, but also provides some flexible power electronic interfaces for renewable energy source access.

The other parts of this paper are organized as follows. Section II presents the topology and mathematical model of the UPQC-QAB. In Section III, the associated control schemes of the three single-phase series converters, the shunt converter and the QAB are proposed. In Section IV, the MATLAB/Simulink simulation results and hardware-in-the-loop testing are presented. Finally, the conclusions are given in Section VI.

II. TOPOLOGY AND MATHEMATICAL MODEL OF UPQC-QAB

In this section, the topology of the QAB-based UPQC is presented and descripted in detail. Besides, the mathematical models of the series converter, the shunt converter and the QAB are introduced.

A. TOPOLOGY OF UPQC-QAB

The circuit configuration of the three-phase UPQC-QAB is shown in Fig. 1, which is composed of three single-phase series converters, a three-phase shunt converter and a QAB converter. Three DC ports (ports a, b and c) of the QAB are connected with the three single-phase series converters, and the fourth one (port d) is connected with the shunt converter. In this topology, the QAB functions as an energy router in the UPQC, and it provides flexible power electronic interfaces for renewable energy sources. For example, ports a, b and c could be the interfaces for photovoltaic panels, where the DC-link voltages could be regulated conveniently. Moreover, the conventional bulky transformer is replaced by small high-frequency ones. Thus, in contrast to the conventional UPQC, the proposed UPQC-QAB has the advantages of higher power density and more flexibility.

Compared with other existing custom compensation devices such as DVR, STATCOM, three-phase UPQC, three single-phase UPQC, and three-phase UPQC-DAB, the features of the UPQC-QAB are listed in Table 1. As shown, apart from the merits of removing the LF transformer and providing more electronics interfaces, the proposed UPQC-QAB has the advantages of mitigation of voltage sag/swell, compensation of load reactive power, elimination of current harmonics and mitigation of unbalanced grid current simultaneously.

B. MODEL OF SERIES CONVERTER

In the UPQC-QAB, the series converter is composed of three single-phase H-bridges. Based on Fig. 1, the mathematic model of single-phase series converter can be expressed as follows:

$$\begin{cases} L_{se}\dfrac{di_{sex}}{dt} = -R_{se}i_{sex} + v_{sex} - v_{ix} \\ C_{se}\dfrac{dv_{sex}}{dt} = i_{5x} - i_{sex} \end{cases} \tag{1}$$

where v_{sex} ($x = a, b, c$) are the injected voltages of series converter, v_{Sx} and i_{Sx} are the grid voltages and phase currents, respectively. i_{sex} represent the inductance currents. v_{ix} are the input voltages of series converter. L_{se} and C_{se} represent the filter inductance and capacitance, and R_{se} is the equivalent resistance.

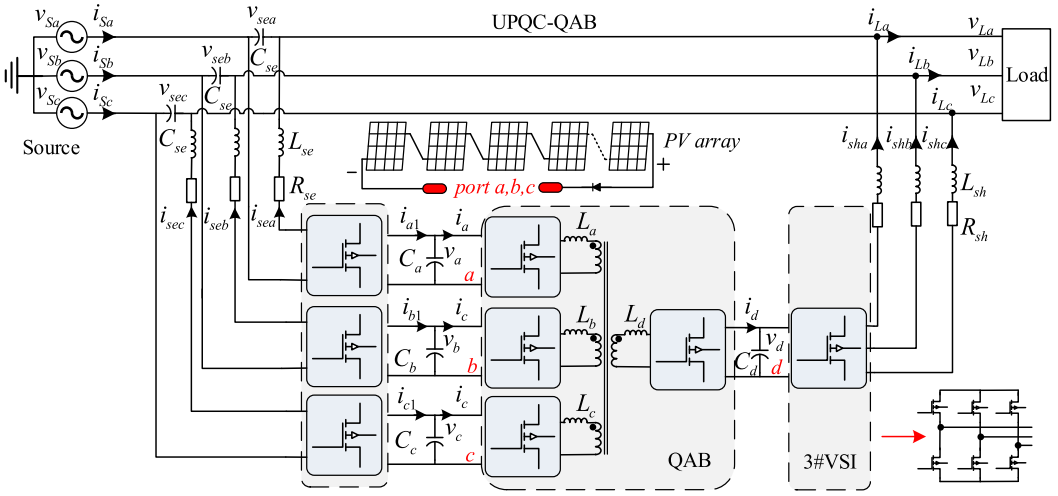

FIGURE 1. Circuit Configuration of three-phase UPQC-QAB.

C. MODEL OF SHUNT CONVERTER

The shunt converter of the UPQC-QAB is a conventional three-phase converter. From Fig. 1, the mathematic model of the shunt converter is descripted as (2),

$$L_{sh}\frac{di_{shx}}{dt} = -R_{sh}i_{shx} + v_{ox} - v_{Lx} \tag{2}$$

where v_{Lx} are the load voltages. v_{ox} are the output voltages of the shunt converter. L_{sh} and R_{sh} represent the filter inductance and equivalent resistance.

D. MODEL OF QAB CONVERTER

The power circuit of the QAB converter is shown in Fig. 1. As shown, $[v_a\ v_b\ v_c\ v_d]^T$ and $[i_a\ i_b\ i_c\ \ i_d]^T$ are the DC-link voltages and input currents of the related ports. $[i_{a1}\ i_{b1}\ \ i_{c1}]^T$ are the output currents of three single-phase series converters at the DC-links. $[L_a\ L_b\ L_c\ L_d]^T$ and $[N_a\ N_b\ N_c\ N_d]^T$ are the leakage inductances and winding turns, respectively. $[C_a\ C_b\ \ C_c\ C_d]^T$ are the DC-link capacitances.

Referring to port d and applying the Kirchhoff's law in "Y" equivalent circuit of the QAB (in Fig. 2(a)), the equivalent link inductance of port m and n [26] is calculated as,

$$L_{mn} = L'_m L'_n \left(\frac{1}{L_a} + \frac{1}{L'_b} + \frac{1}{L'_c} + \frac{1}{L'_d}\right) \tag{3}$$

where $m, n \in \{a, b, c, d\}$ and $m \neq n$. $[L'_a\ L'_b\ L'_c\ L'_d]^T$ are the equivalent leakage inductances referring to port d. Fig. 2(b) shows the "Δ" equivalent circuit of the QAB.

In this study, the phase-shift-modulation (PSM) is used to control the power flow between any two ports. Thus, the QAB is driven by the square-wave voltages generated by their corresponding full-bridge modules with a 50% duty cycle.

The power transferred from port m to port n can be expressed as follows,

$$P_{nn} = \frac{V'_m V'_n}{2f_s L_{mn}} D_{mn}\left(1 - |D_{mn}|\right) \tag{4}$$

where f_s is the switching frequency. D_m and D_n are the phase shift ratios of port m and n, respectively. v'_m and v'_n represent

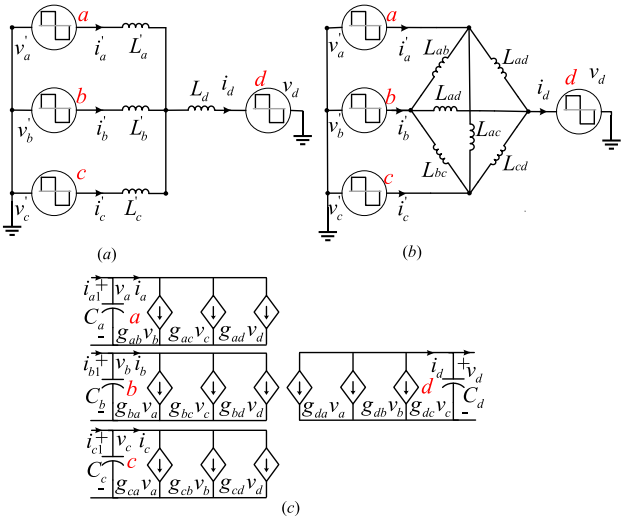

FIGURE 2. Equivalent circuits of the QAB (a) "Y" equivalent circuit; (b) "Δ" equivalent circuit; (c) gyrator-based average model.

the equivalent voltages referring to port d. V'_m and V'_n are the amplitudes of v'_m and v'_n.

Thus, the main waveforms of corresponding voltage of ports m, n and the link-inductor ac current in Fig. 3.

By utilizing Gyrator theory, the gyrator-based average model of QAB [25] can be achieved (in Fig. 2c). Furthermore, the associated gyration gain is given as (5),

$$g_{mn} = \frac{N_d^2}{N_m N_n}\frac{1}{2f_s L_{mn}} D_{mn}\left(1 - |D_{mn}|\right) \tag{5}$$

Thus, the mathematic model of the QAB is given as (6),

$$\begin{cases} C_a\dfrac{dv_a}{dt} = g_{ab}v_b + g_{ac}v_c + g_{ad}v_d - i_{a1} - i_{pva} \\ C_b\dfrac{dv_b}{dt} = g_{ba}v_a + g_{bc}v_c + g_{bd}v_d - i_{b1} - i_{pvb} \\ C_c\dfrac{dv_c}{dt} = g_{ca}v_a + g_{cb}v_b + g_{cd}v_d - i_{c1} - i_{pvc} \end{cases} \tag{6}$$

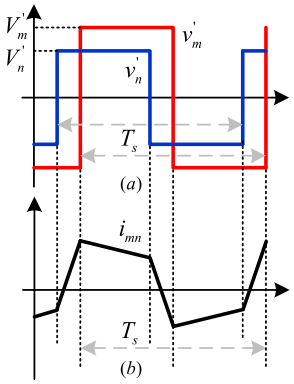

FIGURE 3. Waveforms of the QAB: (*a*) equivalent voltages of ports m, n and (*b*) link-inductor current.

where i_{pvx} represent the output currents of PV array integrated to UPQC-QAB from DC port x. When i_{pvx} is equal to 0, it means that the PV array is disconnected from port x. While i_{pvx} is bigger than 0, it denotes that the PV array operates at UPQC-connected mode.

From (4), the gyration gain g_{mn} is a nonlinear function of the phase shift ratios D_m and D_n. As shown in (5), the original QAB system in Eq. (6) is considered as a three-input three-output nonlinear and strong cross-coupling system.

III. CONTROL SCHEMES OF UPQC-QAB

A. CONTROL OF SERIES CONVERTER

To track the grid angular frequency ω accurately, an adaptive filter is utilized instead of the phase-looked-loop (PLL). The block diagram of the adaptive filter is shown in Fig. 4(*a*).

For the input signal x(n), the adaptive filter provides two signals $x_1(n+1)$ and its quadrature signal $qx_1(n+1)$.

$$\begin{cases} x_1(n+1) = -x_1(n) + \eta(n) \\ qx_1(n+1) = qx_1(n) + \tan\left(\dfrac{\omega_s T_s}{2}\right)\eta(n) \end{cases} \tag{7}$$

$$\eta(n) = \frac{\tan(\frac{\omega_s T_s}{2})\{K_s[x(n)+x(n+1)-2qx_1(n)]+2x_1(n)\}}{1+\tan\left(\frac{\omega_s T_s}{2}\right)\left[K_s+\tan\left(\frac{\omega_s T_s}{2}\right)\right]} \tag{8}$$

where n represents the n-th sampling period, q represents the quadrature shift operator. T_s is the sampling period. The parameter K_s determines the steady-state accuracy and dynamic performance of the adaptive filter. And K_s is chosen as 0.2. ω_s is the resonant frequency, which has been proved that the $\omega_s \equiv \omega$ is the unique exponentially stable equilibrium in the proposed system in [30]. Besides, the detailed description, analysis and proof is shown in [30].

The adaptive law of the adaptive filter is given as

$$\omega_s(n+1) = \omega_s(n) - \gamma \tan\left[\frac{\omega_s(n)T_s}{2}\right]\cdot[x(n)-x_1(n)]\cdot qx_1(n) \tag{9}$$

where the parameter γ is given as 0.0001 in this study. In [30], by using the averaging theory, it has been proven that

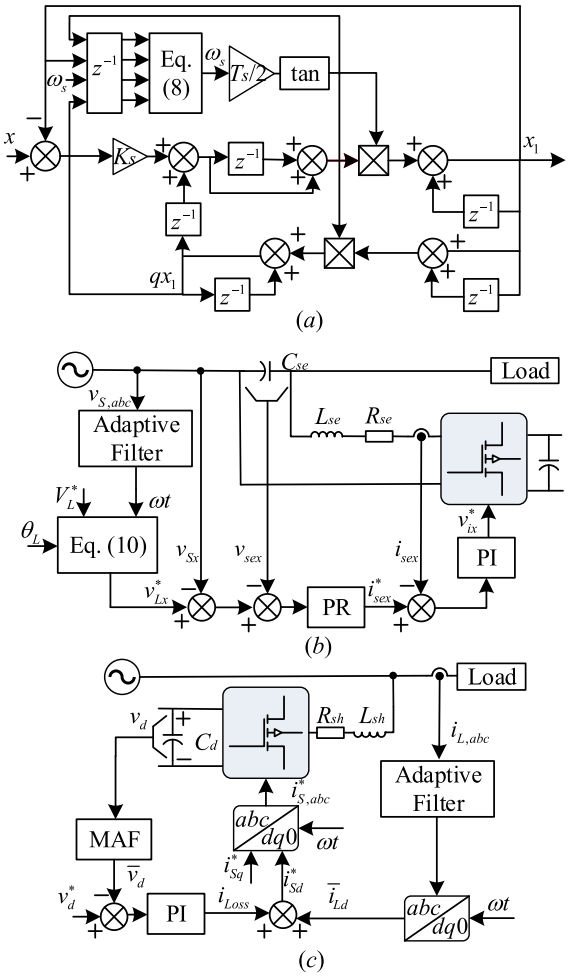

FIGURE 4. Control block diagram for (a) the adaptive filter, (b) the series converter and (c) the shunt converter.

the control law of Eq. (9) has the exponential convergence property as long as γ is small enough and greater than zero. Thus, the parameter γ should be relatively small to ensure the stability.

The control targets of series converters of UPQC-QAB is to maintain the load voltage at the desire value. The reference load phase-voltages v_{Lx}^* are given as

$$\begin{cases} v_{La}^* = V_L^* \sin(\omega t + \theta_L) \\ v_{Lb}^* = V_L^* \sin(\omega t + \theta_L - 2\pi/3) \\ v_{Lc}^* = V_L^* \sin(\omega t + \theta_L + 2\pi/3) \end{cases} \tag{10}$$

where V_L^* and θ_L are the reference amplitude value and phase angle of the load reference voltage.

Furthermore, the reference series injected voltage is given as,

$$v_{sex}^* = v_{Lx}^* - v_{Sx} \tag{11}$$

Fig. 4(*b*) shows the control block diagram for the single-phase series converter. To realize the dynamic voltage compensation of the negative sequence and harmonics components, the voltage loop design method based on

proportional resonant (PR) controller is utilized. Finally, the outputs of PR controller i^*_{sex} and sensed currents i_{sex} are sent to the inner current controller for the PWM signals generation of the single-phase series converter.

B. CONTROL OF SHUNT CONVERTER

The control objectives of the shunt converters are to 1) maximize the power factor of power grid, 2) mitigate the load current harmonics and 3) maintain the voltage v_d at a desired value.

To obtain the desired grid current reference, the d-axis component of reference grid current is determined by (12),

$$i^*_{Sd} = \bar{i}_{Ld} + i_{Loss} \tag{12}$$

where $\bar{i}_{Ld}$ is the fundament component of d-axis component of sensed load current $i_{L,abc}$. By using the proposed adaptive filter, the fundament component $\bar{i}_{L,abc}$ of $i_{L,abc}$ can be achieved. Next, the component $\bar{i}_{Ld}$ can be gained by utilizing $abc/dq0$ transformation. i_{Loss} represents the loss component, which is the output of the PI controller of DC-link at port d. Since the sensed DC-link voltage v_d contains noise and ripples, it is necessary to filter the voltage v_d to improve the dynamic performance of the shunt controller. To extract the fundament component of v_d, the moving average filter (MAF) is utilized, which has shown good performance in extracting the DC components in [31].

The detailed discuss and analysis of MAF can be seen in [31]. The transfer function of MAF is given as (13),

$$f_{MAF}(s) = \frac{1 - e^{-T_\omega s}}{T_\omega s} \tag{13}$$

where T_ω represents the window length of MAF.

Fig. 4(c) shows the control block diagram for the shunt converter. After obtaining the reference grid current i^*_{Sd}, three-phase reference grid currents $i^*_{S,abc}$ could be gained by utilizing the $dq0/abc$ transformation. Finally, the errors between $i^*_{S,abc}$ and $i_{S,abc}$ are sent to the PWM controller for the gate signals generation of the shunt converter.

C. CONTROL OF QAB CONVERTER

Because the QAB functions as an energy router in the UPQC-QAB, it aims to realize the active power flow between three single-phase series converters (port a, b, c) and three-phase shunt converter (port d).

For convenience, (6) could be linearized around the operation point. Thus, the mathematic model of the QAB can be rewritten as follows by some manipulation.

$$C_x \frac{dv_x}{dt} \approx D_x \sum_{n\neq x} (k_{xn} v_n) - \sum_{n\neq x} \left(k_{xn} v_n D^*_n\right) - i_{x1} - i_{pvx} \tag{14}$$

where

$$k_{xn} = \frac{N_d^2}{N_x N_n} \frac{1}{2 f_s L_{xn}}, \quad (n = a, b, c, d \text{ and } n \neq x).$$

Furthermore, (14) could be written as follows,

$$C_x \frac{dv_x}{dt} \approx k_x D_x + \xi \tag{15}$$

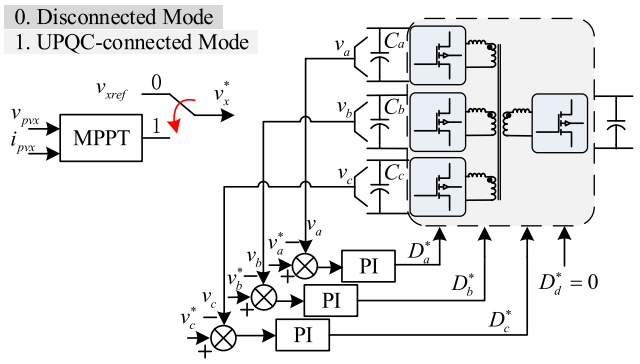

FIGURE 5. Control block diagram for the QAB converter.

where

$$k_x = \sum_{n=x} (k_{xn} v_n), \; \xi = -\sum_{n\neq x} \left(k_{xn} v_n D^*_n\right) - i_{x1} - i_{pvx}$$

where ξ represents the disturbance.

Thus, the reference phase shift ratios could be obtained by utilizing the PI controllers, which is given as (16)

$$D^*_x = \left(K_{qp} + \frac{K_{qi}}{s}\right)\left(v^*_x - v_x\right) \quad (x = a, b, c) \tag{16}$$

where K_{qp} and K_{qi} are the gains of the PI controller, respectively. v^*_x represents the reference voltages of the DC port. When the PV array is connected to the UPQC-QAB from DC port x, the reference port voltage v^*_x can be achieved by using the maximum power point tracking (MPPT) controller [15]. Otherwise, when PV array is disconnected, the reference port voltage is given as v_{xref}.

Fig. 5 shows the control block diagram of the QAB. As seen, the errors between the reference and measured DC-link voltages of port x are sent to the PI controllers to obtain the reference phase shift ratios $[D^*_a\ D^*_b\ D^*_c]^T$. Finally, the corresponding reference phase shift ratios are sent to the PSM controllers for the gate signals generation of the QAB.

IV. VERIFICATIONS

To elaborate and validate the proposed topology and control schemes, the MATLAB/Simulink simulations and hardware-in-the-loop testing have been carried out on the three-phase UPQC-QAB. Table 2 lists the parameters involved in the simulations. The switching frequencies of the control schemes of the series converter, the shunt converter and the QAB converter are assigned to be 20kHz, 20kHz and 100kHz. Besides, the UPQC-P method is utilized in this study, where the series converter only injects/absorbs the active power to/from the power grid [13].

A. SIMULATION RESULTS

In this section, the MATLAB/Simulink simulation results of the UPQC-QAB are illustrated. To comprehensively test the compensation performance of the UPQC-QAB, four case studies with different grid voltages and load scenarios are presented, where the detailed parameters are listed in Table 3.

TABLE 2. Parameters used in the simulations.

Symbol	Description	Value
v_{Sabc}	Grid phase voltage	230V(rms)
ω	Grid angular frequency	314rad/s
L_{se}	Series filter inductance	1.5mH
C_{se}	Series filter capacitance	50μF
R_{se}	Series equivalent resistance	0.02Ω
L_{sh}	Shunt filter inductance	2mH
R_{sh}	Shunt equivalent resistance	0.02Ω
v_{abc}	DC-link voltage of port *abc*	400V
v_d	DC-link voltage of port *d*	800V
C_{abc}	Capacitance of port *abc*	1000μF
C_d	Capacitance of port *abc*	6000μF
L_{abc}	Leakage inductance of port *abc*	6.75μH
L_d	Leakage inductance of port *d*	27μH
N_{abc}	Winding turns of port *abc*	1
N_d	Winding turns of port *d*	2

TABLE 3. Grid voltage and load states during four case studies.

	Grid voltage	Load
Case 1	Balanced voltage sag/swell	R_a=12.7Ω, L_a=30.3mH; R_b=12.7Ω, L_b=30.3mH; R_c=12.7Ω, L_c=30.3mH;
Case 2	Unbalanced voltage sag/swell	R_a=12,7Ω, L_a=30.3mH; R_b=6Ω, L_b=40mH; R_c=18Ω, L_c=20mH; Rectifier R=100Ω, L=60mH;
Case 3	Distorted grid voltage	R_a=12,7Ω, L_a=30.3mH; R_b=6Ω, L_b=40mH; R_c=18Ω, L_c=20mH; Rectifier R=100Ω, L=60mH;
Case 4	Balanced voltage sag/swell	R_a=12.7Ω, L_a=30.3mH; R_b=12.7Ω, L_b=30.3mH; R_c=12.7Ω, L_c=30.3mH;

1) CASE STUDY 1

Firstly, the performance of the UPQC-QAB prototype is tested in terms of mitigation of three-phase balanced voltage sag/swell, and compensation of the load reactive power.

Fig. 6 shows the simulation waveforms of the UPQC-QAB under case study 1. As shown in Fig. 6 (*a*), three-phase balanced voltage sag happens between 0.12 and 0.16 s with a depth of 20%, and three-phase balanced voltage swell with a depth of 20% happens during 0.16s and 0.20s. With the compensation of series converters (in Fig. 6 (*c*)), the load voltage v_L is always kept balanced and maintained at the desired value (seen in Fig. 6 (*b*)). From Fig. 6(*d*)-(*f*), the grid current i_S is balanced and in-phase with grid voltage by injecting the shunt current i_{sh}. Besides, all the four DC-link voltages are at the corresponding desired values in Fig. 6(*g*)-(*h*).

Fig. 7 shows the related simulation waveforms of load active/reactive power (P_L/Q_L), the grid active/reactive power (P_S/Q_S), the series injected active/reactive power (P_{se}/Q_{se}) and the shunt injected active/reactive power (P_{sh}/Q_{sh}). As shown, the load active power (8kW) is totally provided by the grid, and the load reactive power (6kW) is totally provided by the shunt converter.

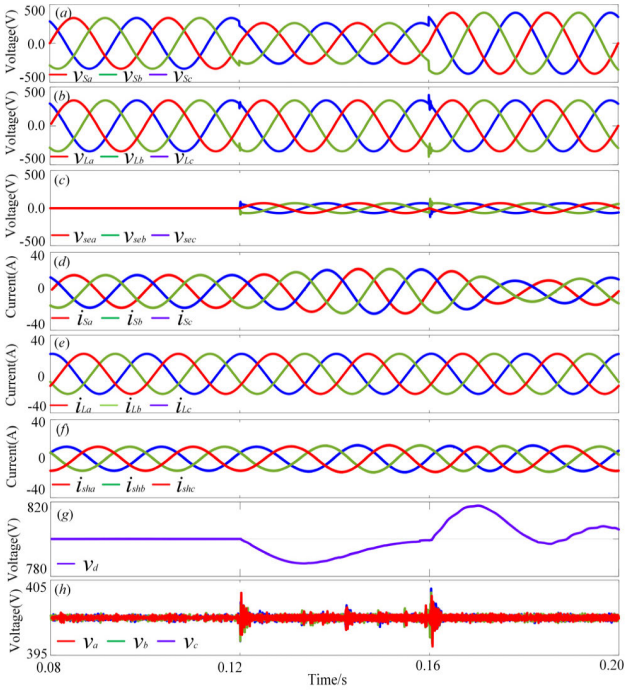

FIGURE 6. Waveforms of v_S, v_L, v_{se}, i_S, i_L, i_{sh}, v_a, v_b, v_c and v_d of UPQC-QAB under case study 1.

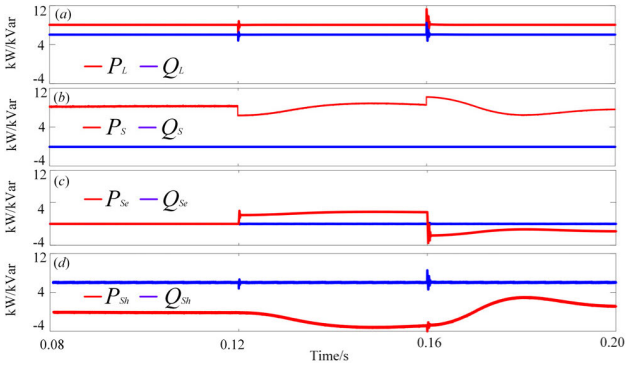

FIGURE 7. Waveforms of P_L, Q_L, P_S, Q_S, P_{se}, Q_{se}, P_{sh} and Q_{sh} of UPQC-QAB under case study 1.

2) CASE STUDY 2

Secondly, the case study 2 is designed to test the capabilities of the UPQC-QAB in mitigation of unbalanced voltage sag, compensation of both reactive power, and elimination of current harmonics.

Fig. 8 shows the simulation waveforms of the UPQC-QAB under case study 2. In Fig. 8(a), the single-phase (*c*-phase) grid voltage sag occurs during 0.12s and 0.16s with a depth of 40%, and three-phase unbalanced voltage sag occurs between 0.16s and 0.20s (the sag depths of v_{Sa}, v_{Sb} and v_{Sc} are 20%, 15% and 25%, respectively). From Fig. 8(*b*)-(*c*), with the compensation of three single-phase series converters, the three-phase load voltages are almost kept unchanged. As seen

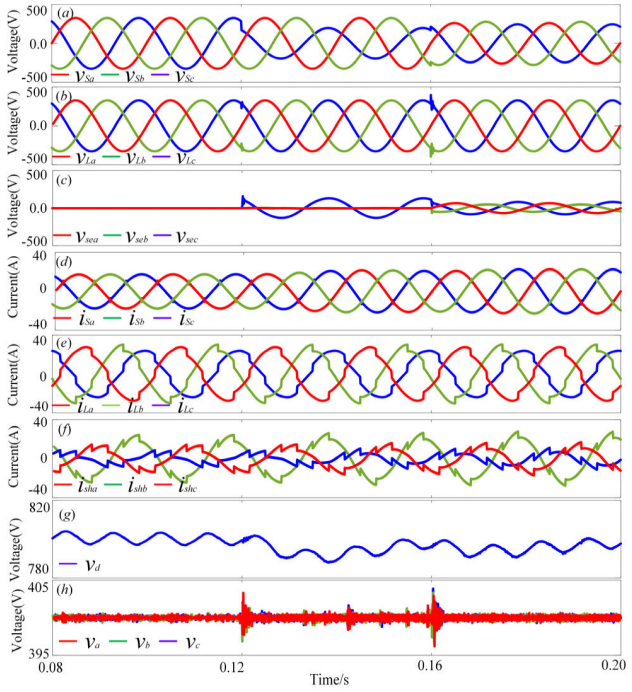

FIGURE 8. Waveforms of v_S, v_L, v_{se}, i_S, i_L, i_{sh}, v_a, v_b, v_c and v_d of UPQC-QAB under case study 2.

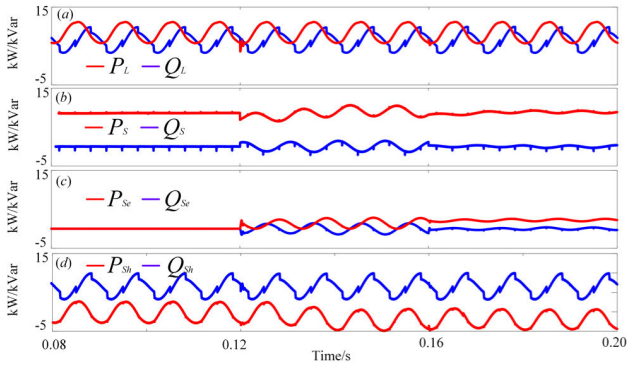

FIGURE 9. Waveforms of P_L, Q_L, P_S, Q_S, P_{se}, Q_{se}, P_{sh} and Q_{sh} of UPQC-QAB under case study 2.

from Fig. 8(*e*), the load current contains lots of harmonics, where the total harmonic distortion (THD) is about 8.56%. Fig. 8(*d*) shows the grid current. As seen, the current is balanced and in-phase with grid voltage and its THD is 2.06%. Fig. 8(*f*) shows the injected shunt current i_{sh} through the shunt converter. Besides, all the DC-link voltages are around the desired values with small pulsations in Fig. 8(*g*)- (*h*).

Fig. 9 shows the related simulation power waveforms of UPQC-QAB in case 2. As shown, since both the three-phase loads are unbalanced and the grid voltage are unbalanced, the series and shunt injected power are also unbalanced.

3) CASE STUDY 3

In this case, the UPQC-QAB operates under distorted grid voltage sag/swell and nonlinear loads.

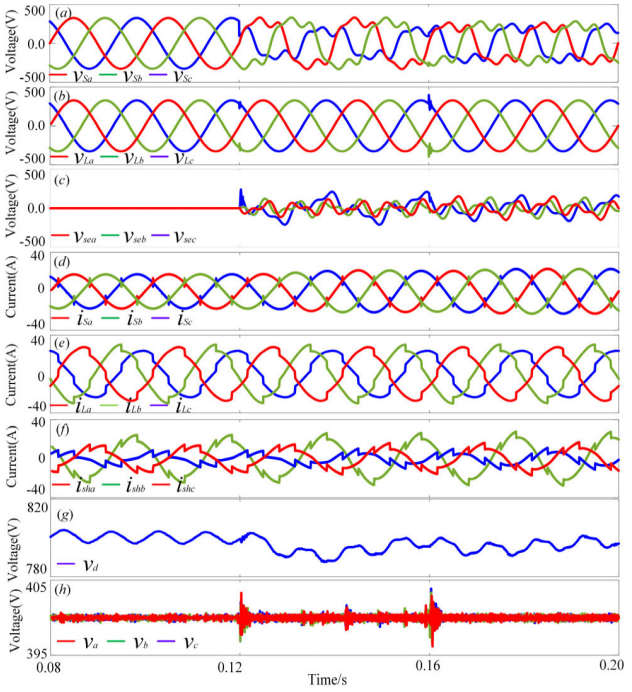

FIGURE 10. Waveforms of v_S, v_L, v_{se}, i_S, i_L, i_{sh}, v_a, v_b, v_c and v_d of UPQC-QAB under case study 3.

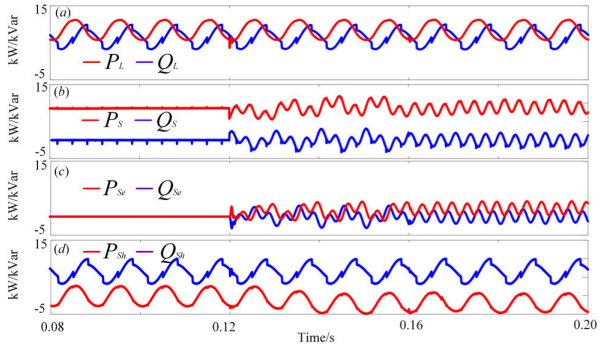

FIGURE 11. Waveforms of P_L, Q_L, P_S, Q_S, P_{se}, Q_{se}, P_{sh} and Q_{sh} of UPQC-QAB under case study 3.

The simulation waveforms of the UPQC-QAB under this case are shown in Fig. 10. As seen in Fig. 10(*a*), the grid voltage is distorted and unbalanced in the time interval (0.12s, 0.20s), where the total harmonic distortion is 25%. Due to the compensation of the UPQC-QAB (in Fig. 10(*c*)), the load voltage is kept balanced, and the THD is 0.74% (shown in Fig. 10(*b*)). From Fig. 10(*d*)-(*f*), the grid current i_S is balanced and in-phase with grid voltage by injecting the shunt current i_{sh} through the shunt converter. And all the DC-link voltages at all DC ports are shown in Fig. 10(*g*)-(*h*).

The related simulation power waveforms of UPQC-QAB in case 3 are shown in Fig. 11(*a*)-(*d*). As shown, because the grid voltage are distorted, the series injected active/reactive power also have pulsations.

4) CASE STUDY 4

Finally, the performance of the UPQC-QAB integrated with PV arrays is tested, and the grid voltage and load scenarios are

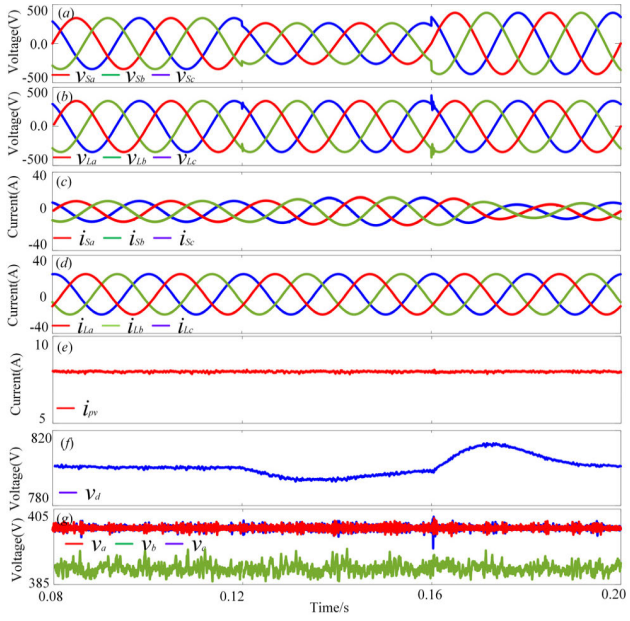

FIGURE 12. Waveforms of v_S, v_L, i_S, i_L, i_{pv}, v_b and v_d of UPQC-QAB under case study 4.

the same with case study 1. The related simulation waveforms are shown in Fig. 12. The voltage at the maximum power point is 387V and the current at the maximum power point is given as 8A.

As shown in Fig. 12(a)-(b), the load voltage v_L is always kept balanced and at the desired value because of the compensation of UPQC-QAB. The grid current i_S (shown in Fig. 12(c)) is also balanced and in-phase with grid voltage.

Fig. 12(e) shows the output current of PV array i_{pv}. As seen, due to the integration with PV array, the grid current decreases, which means that the power grid and the PV array supply the load active power together. Besides, the DC voltage v_b of port b (which connects to the PV array) is still kept stable and v_d has a smaller pulsation (around the voltage 387 V at the maximum power of PV array) in contrast to case study 1 (in Fig. 12(f)-(g)).

The related simulation power waveforms of UPQC-QAB in case 4 are shown in Fig. 13(a)-(f). As shown, the active power generated by PV arrays is about 3kW and supplies the load from the shunt converter. Thus, the active power is decreased to 5kW from 8kW. Besides, due to reduced grid active power, the grid currents and series injected active power will be reduced when compared with case 1.

B. HARDWARE-IN-THE_LOOP TESTING

Furthermore, the proposed control schemes are verified with OPAL-RT 4510. The physical models of the UPQC-QAB and the power systems, including the source, the loads, etc., are built in the real-time digital simulator of the OPAL-RT 4510. The sampling time of the real-time digital simulator is set to 1μs. Besides, in this test, the root mean square (RMS) value of grid phase voltage is 57.7V. The three-phase loads are given as: $R_a = 6\Omega$, $L_a = 10$mH; $R_b = 8\Omega$, $L_b = 9$mH;

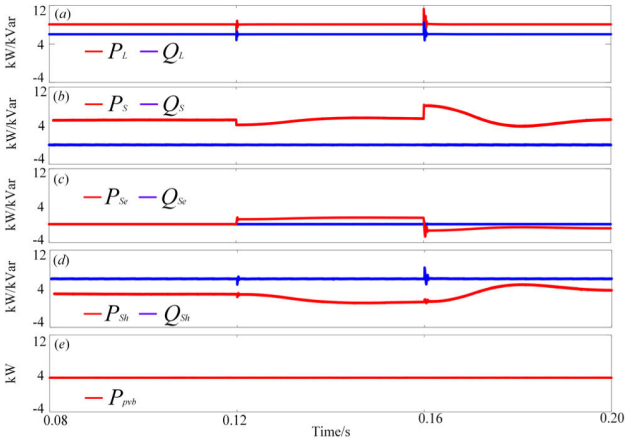

FIGURE 13. Waveforms of P_L, Q_L, P_S, Q_S, P_{se}, Q_{se}, P_{sh}, Q_{sh} and P_{pvb} of UPQC-QAB under case study 4.

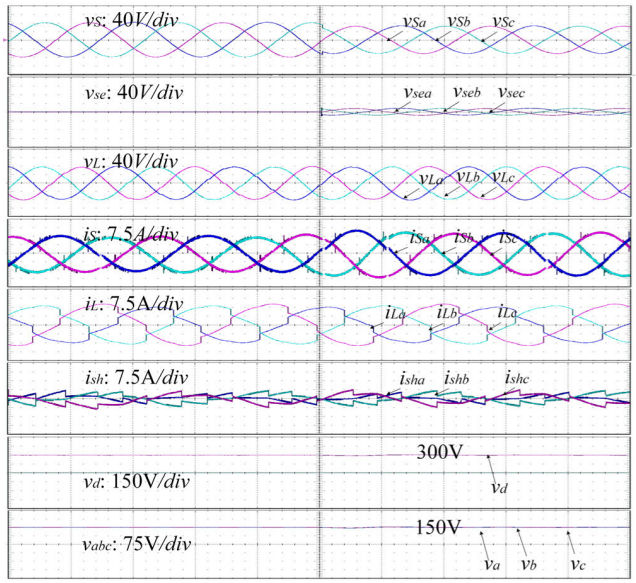

FIGURE 14. Waveforms of v v_S, v_L, v_{se}, i_S, i_L, i_{sh}, v_a, v_b, v_c and v_d of UPQC-QAB under nonlinear load and balanced grid voltage sag.

$R_c = 7\Omega$, $L_c = 8$mH; and diodes rectifier load $R = 20\Omega$, $L = 20$mH. The results of the hardware-in-the-loop testing of UPQC-QAB are presented in Fig. 14-16.

1) OPERATION UNDER NONLINEAR LOADS AND BALANCED GRID VOLTAGES SAG

The waveforms of the UPQC-QAB under nonlinear load and balanced grid voltage sag are illustrated in Fig. 14. As shown, the grid voltage v_S changes from the normal state to 20% sag state, the load voltage v_L is almost kept unchanged by injecting the voltage v_{se} through the series converter. Besides, due to the compensation of shunt converter, the grid current i_S is always balanced and in-phase with grid voltage, and the current harmonics are also mitigated. Moreover, four DC-link voltages (v_a, v_b, v_c and v_d) are at the corresponding desired values.

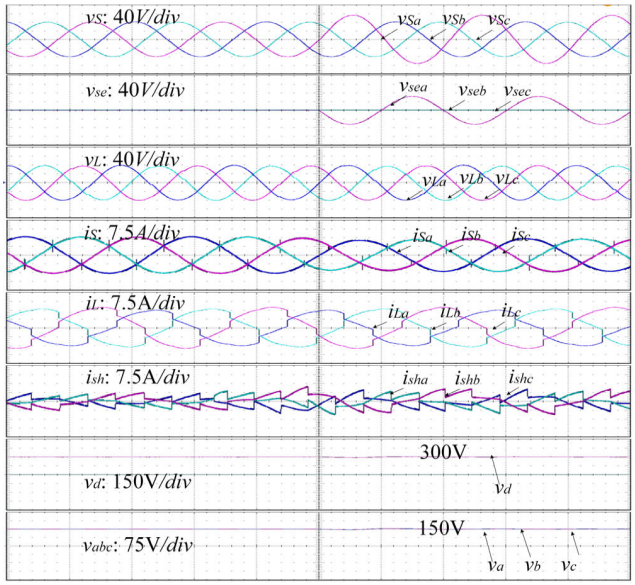

FIGURE 15. Waveforms of v_S, v_L, v_{se}, i_S, i_L, i_{sh}, v_a, v_b, v_c and v_d of UPQC-QAB under nonlinear load and unbalanced grid voltage.

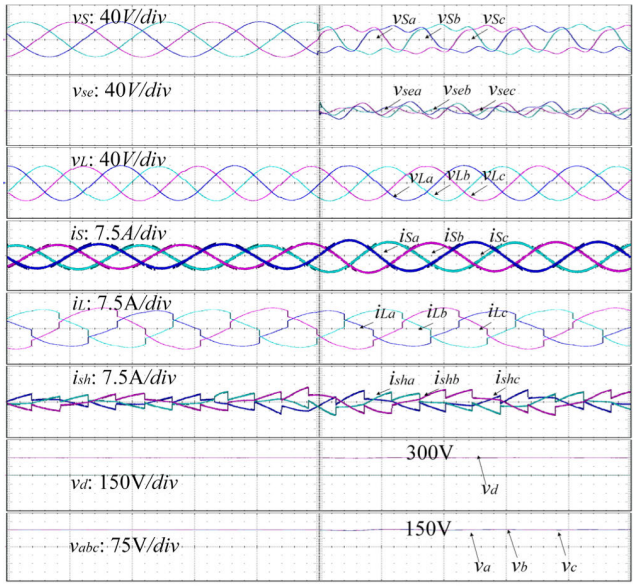

FIGURE 16. Waveforms of v_S, v_L, v_{se}, i_S, i_L, i_{sh}, v_a, v_b, v_c and v_d of UPQC-QAB under nonlinear load and distorted grid voltage.

2) OPERATION UNDER NONLINEAR LOADS AND UNBALANCED GRID VOLTAGES

Fig. 15 illustrates the waveforms of the UPQC-QAB under nonlinear load and unbalanced grid voltage. As shown, the grid voltage v_S changes from the normal state to the a-phase voltage sag state, the load voltage v_L is maintained balanced and at the rated value by injecting the voltage v_{se}. By injecting the current i_{sh} through the shunt converter, the grid current i_S is maintained balanced and in-phase with grid voltage.

3) OPERATION UNDER NONLINEAR LOAD AND DISTORTED GRID VOLTAGES

The waveforms of the UPQC-QAB under nonlinear load and distorted grid voltage are illustrated in Fig. 16. As shown, the grid voltage v_S changes from the normal state to the distorted state, the load voltage v_L also remains unchanged by injecting the voltage v_{se}. By injecting the current i_{sh} through the shunt converter, the grid current i_S is maintained balanced and in-phase with grid voltage.

V. CONCLUSION

In this study, a topology of UPQC integrated with the QAB is proposed. Due to the removal of the bulky low frequency isolation transformers and the use of the QAB, the UPQC-QAB has the advantages of higher power density and more flexibility. Besides, the unbalanced grid currents caused by the unbalanced load can be mitigated compared with three-phase UPQC made up of three single-phase UPQCs. The effectiveness of the UPQC-QAB were evaluated under distorted grid voltage, balanced/unbalanced grid voltage sag/swell, unbalanced and nonlinear load conditions.

Because of the lower investment cost, smaller size and more power electronic interfaces, the UPQC-QAB may be widely used in residential areas or families. Furthermore, under the topology of proposed UPQC-QAB, some promising work can be done in the future, including: 1) the optimal VA capacity design of the UPQC-QAB; 2) the optimal operation of the UPQC-QAB; and 3) the UPQC-QAB integrated with renewable energy sources (photovoltaic panels, fuel cell, battery and so on).

REFERENCES

[1] M. Bollen and F. Hassan, *Integration of Distributed Generation in the Power System: Power Quality Disturbances*. Hoboken, NJ, USA: Wiley, 2011, pp. 223–298.

[2] R. Fehr, *Industrial Power Distribution: Power Quality*. Hoboken, NJ, USA: Wiley, 2016, pp. 335–356.

[3] X. Liang, "Emerging power quality challenges due to integration of renewable energy sources," *IEEE Trans. Ind. Appl.*, vol. 53, no. 2, pp. 855–866, Mar. 2017.

[4] R. I. Bojoi, L. R. Limongi, D. Roiu, and A. Tenconi, "Enhanced power quality control strategy for single-phase inverters in distributed generation systems," *IEEE Trans. Power Electron.*, vol. 26, no. 3, pp. 798–806, Mar. 2011.

[5] Z. Zeng, H. Yang, S. Tang, and R. Zhao, "Objective-oriented power quality compensation of multifunctional grid-tied inverters and its application in microgrids," *IEEE Trans. Power Electron.*, vol. 30, no. 3, pp. 1255–1265, Mar. 2015.

[6] Z. Zeng, H. Li, S. Tang, H. Yang, and R. Zhao, "Multi-objective control of multi-functional grid-connected inverter for renewable energy integration and power quality service," *IET Power Electron.*, vol. 9, no. 4, pp. 761–770, Mar. 2016.

[7] X. Sun, R. Han, H. Shen, B. Wang, Z. Lu, and Z. Chen, "A double-resistive active power filter system to attenuate harmonic voltages of a radial power distribution feeder," *IEEE Trans. Power Electron.*, vol. 31, no. 9, pp. 6203–6216, Sep. 2016.

[8] J. Fang, G. Xiao, X. Yang, and Y. Tang, "Parameter design of a novel series-parallel-resonant LCL filter for single-phase half-bridge active power filters," *IEEE Trans. Power Electron.*, vol. 32, no. 1, pp. 200–217, Jan. 2017.

[9] D. Somayajula and M. L. Crow, "An integrated dynamic voltage restorer-ultracapacitor design for improving power quality of the distribution grid," *IEEE Trans. Sustain. Energy*, vol. 6, no. 2, pp. 616–624, Apr. 2015.

[10] A. Benali, M. Khiat, T. Allaoui, and M. Denai, "Power quality improvement and low voltage ride through capability in hybrid wind-PV farms grid-connected using dynamic voltage restorer," *IEEE Access*, vol. 6, pp. 68634–68648, 2018.

[11] H. Fujita and H. Akagi, "The unified power quality conditioner: The integration of series- and shunt-active filters," *IEEE Trans. Power Electron.*, vol. 13, no. 2, pp. 315–322, Mar. 1998.
[12] V. Khadkikar and A. Chandra, "UPQC-S: A novel concept of simultaneous voltage sag/swell and load reactive power compensations utilizing series inverter of UPQC," *IEEE Trans. Power Electron.*, vol. 26, no. 9, pp. 2414–2425, Sep. 2011.
[13] V. Khadkikar, "Enhancing electric power quality using UPQC: A comprehensive overview," *IEEE Trans. Power Electron.*, vol. 27, no. 5, pp. 2284–2297, May 2012.
[14] S. K. Khadem, M. Basu, and M. F. Conlon, "Intelligent islanding and seamless reconnection technique for microgrid with UPQC," *IEEE J. Emerg. Sel. Topics Power Electron.*, vol. 3, no. 2, pp. 483–492, Jun. 2015.
[15] L. B. G. Campanhol, S. A. O. da Silva, A. A. de Oliveira, and V. D. Bacon, "Power flow and stability analyses of a multifunctional distributed generation system integrating a photovoltaic system with unified power quality conditioner," *IEEE Trans. Power Electron.*, vol. 34, no. 7, pp. 6241–6256, Jul. 2019.
[16] A. K. Jindal, A. Ghosh, and A. Joshi, "Interline unified power quality conditioner," *IEEE Trans. Power Del.*, vol. 22, no. 1, pp. 364–372, Jan. 2007.
[17] J. A. Munoz, J. R. Espinoza, L. A. Moran, and C. R. Baier, "Design of a modular UPQC configuration integrating a components economical analysis," *IEEE Trans. Power Del.*, vol. 24, no. 4, pp. 1763–1772, Oct. 2009.
[18] Q. Xu, F. Ma, A. Luo, Z. He, and H. Xiao, "Analysis and control of M3C-based UPQC for power quality improvement in medium/high-voltage power grid," *IEEE Trans. Power Electron.*, vol. 31, no. 12, pp. 8182–8194, Dec. 2016.
[19] A. Mannan Rauf, A. Vilas Sant, V. Khadkikar, and H. H. Zeineldin, "A novel ten-switch topology for unified power quality conditioner," *IEEE Trans. Power Electron.*, vol. 31, no. 10, pp. 6937–6946, Oct. 2016.
[20] Y. Zhang, S. Zhang, and J. Chen, "The applications of bidirectional full-bridge DC-DC isolated converter in UPQC," in *Proc. Int. Conf. Electr. Mach. Syst.*, Oct. 2008, pp. 1916–1921.
[21] W. Tongzhen and Z. Jin, "Topology and control strategy of UPQC based on high frequency isolation DC/DC converter," in *Proc. 9th IEEE Conf. Ind. Electron. Appl.*, Jun. 2014, pp. 167–172.
[22] G. Buticchi, M. Andresen, M. Wutti, and M. Liserre, "Lifetime-based power routing of a quadruple active bridge DC/DC converter," *IEEE Trans. Power Electron.*, vol. 32, no. 11, pp. 8892–8903, Nov. 2017.
[23] L. F. Costa, G. Buticchi, and M. Liserre, "Quadruple active bridge DC-DC converter as the basic cell of a modular smart transformer," in *Proc. IEEE Appl. Power Electron. Conf. Expo. (APEC)*, Mar. 2016, pp. 2449–2456.
[24] L. F. Costa, G. Buticchi, and M. Liserre, "Quad-active-bridge DC–DC converter as cross-link for medium-voltage modular inverters," *IEEE Trans. Ind. Appl.*, vol. 53, no. 2, pp. 1243–1253, Mar. 2017.
[25] S. Falcones, R. Ayyanar, and X. Mao, "A DC–DC multiport-converter-based solid-state transformer integrating distributed generation and storage," *IEEE Trans. Power Electron.*, vol. 28, no. 5, pp. 2192–2203, May 2013.
[26] P. Frutos, F. Briz, A. Sanchez, and J. M. Guerrero, "Quad-active-bridge as the basic cell of a MMC based SST for DER and des. integration," in *Proc. IEEE 28th Int. Symp. Ind. Electron. (ISIE)*, Jun. 2019, pp. 2349–2355.
[27] Y. Lu, G. Xiao, X. Wang, F. Blaabjerg, and D. Lu, "Control strategy for single-phase transformer-ESS three-leg unified power quality conditioner based on space vector modulation," *IEEE Trans. Power Electron.*, vol. 31, no. 4, pp. 2840–2849, Apr. 2016.
[28] L. F. C. Monteiro, M. Aredes, J. G. Pinto, B. F. Exposto, and J. L. Afonso, "Control algorithms based on the active and non-active currents for a UPQC without series transformers," *IET Power Electron.*, vol. 9, no. 9, pp. 1985–1994, Jul. 2016.
[29] T. Koroglu, A. Tan, M. M. Savrun, M. U. Cuma, K. C. Bayindir, and M. Tumay, "Implementation of a novel hybrid UPQC topology endowed with an isolated bidirectional DC–DC converter at DC link," *IEEE J. Emerg. Sel. Topics Power Electron.*, vol. 8, no. 3, pp. 2733–2746, Sep. 2020.
[30] F. Tedesco, A. Casavola, and G. Fedele, "Unbiased estimation of sinusoidal signal parameters via discrete-time frequency-locked-loop filters," *IEEE Trans. Autom. Control*, vol. 62, no. 3, pp. 1484–1490, Mar. 2017.
[31] R. Pena-Alzola, D. Campos-Gaona, P. F. Ksiazek, and M. Ordonez, "DC-link control filtering options for torque ripple reduction in low-power wind turbines," *IEEE Trans. Power Electron.*, vol. 32, no. 6, pp. 4812–4826, Jun. 2017.

JIAN HAN was born in Hubei, China, in 1993. He received the B.S. degree in electronic engineering from China Three Gorges University, Yichang, China, in 2015. He is currently pursuing the Ph.D. degree in electronic engineering with the Hunan University, Changsha.

His research interests include power quality, FACTs, and matrix converter.

XING LI was born in Hunan, China, in 1988. She received the B.S. and Ph.D. degrees from Central South University, Changsha, China, in 2009 and 2014, respectively.

She is currently an Associate Professor with the College of Electrical and Information Engineering, Hunan University, Changsha. Her research interests include power electronic converter and wind energy conversion systems.

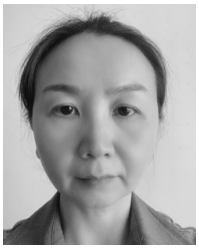

YAN JIANG was born in Hunan, China, in 1972. She received the master's and Ph.D. degrees from Hunan University, Changsha, in 1999 and 2013, respectively.

She is currently an Associate Professor with the College of Electrical and Information Engineering, Hunan University, Changsha. Her research interests include wind energy conversion systems, Information processing, and motor control technology.

SHAONAN GONG was born in Shanxi, China, in 1996. He received the B.S. degree in electrical engineering from Yanshan University, Qinhuangdao, China, in 2019. He is currently pursuing the M.S. degree with the College of Electrical and Information Engineering, Hunan University, Changsha, China.

His research interest includes modeling and control of power electronics converters.